RESEARCH ARTICLE

Renal-Clearable Duplex Optical Reporter for Real-time Imaging of Contrast-induced Acute Kidney Injury

Jiaguo Huang, Yan Lyu, Jingchao Li, Penghui Cheng, Yuyan Jiang, and Kanyi Pu*

Abstract: Contrast-induced acute kidney injury (CIAKI) is a serious medical complication manifested by a rapid deterioration in renal function after administration of contrast medium into patients. Despite its high morbidity and mortality, CIAKI remains a diagnostic dilemma due to its reliance on *in vitro* detection of insensitive late-stage blood and urinary biomarkers. We herein report the synthesis of an activatable duplex reporter (ADR) for real-time *in vivo* imaging of CIAKI. ADR is equipped with chemiluminescence and near-infrared fluorescence (NIRF) signaling channels that can be activated by oxidative stress (superoxide anion, $O_2^{\bullet-}$) and lysosomal damage (*N*-acetyl-β-D-glucosaminidase, NAG), respectively. By virtue of its high renal clearance efficiency (80% injected doses after 24 h injection), ADR detects sequential upregulation of $O_2^{\bullet-}$ and NAG in the kidneys of living mice prior to a significant decrease in glomerular filtration rate (GFR) and tissue damage in the course of CIAKI. This active sensing mechanism allows ADR to outperform the typical clinical assays and detect CIAKI by at least 8 h (NIRF) and up to 16 h (chemiluminescence) earlier. Thus, this study provides new opportunities for real-time noninvasive monitoring of kidney function at the molecular level.

Introduction

Acute kidney injury (AKI) is a life-threatening disorder manifested by a sudden decrease in kidney function and is responsible for an estimated 2 million deaths annually worldwide.[1] Among various etiologies, administration of contrast media is a common contributor to AKI, because contrast media are exclusively eliminated by the kidneys and often induce adverse effects including altered renal hemodynamics and tubular epithelial cell toxicity.[2-3] As over 30 million doses of iodinated contrast media are administered annually for diagnostic imaging and interventional procedure, contrast-induced AKI (CIAKI) has become the third leading cause of hospital-acquired AKI.[4] Therefore, CIAKI is a serious medical complication that demands timely preventive and therapeutic strategies.[5]

In vitro diagnostic methods have been undertaken to monitor renal function upon administration of contrast media so as to prevent CIAKI. In clinic, CIAKI is diagnosed by an increase of >25% serum creatinine (sCr) within 48-72 h of administration of a contrast medium.[6] However, sCr is an insensitive indicator of late-stage kidney dysfunction because it only increases after a 50% decrease in glomerular filtration rate (GFR).[7] Besides, blood and urinary biomarkers such as cystatin C, neutrophil gelatinase-associated lipocalin (NGAL) and kidney injury molecule‑1 (KIM‑1) are under preclinical/clinical trials for detection of CIAKI.[8-9] However, detection of these biomarkers is limited by in vitro diagnostic methods based on static analysis, which are difficult for the longitudinal monitoring of dysregulation in kidneys.[10]

Molecular optical imaging offers a noninvasive way to real-time detect the onset and progression of diseases in living organisms at high spatiotemporal resolution,[11-16] and thus has promise for in-situ monitoring of molecular events in the kidneys. However, only few optical imaging agents including the CdSe/ZnS core-shell quantum dots,[17] silica Cornell dots[18] and the zwitterionic fluorophore ZW800-CDPL[19] are reported to go through renal clearance, and they have not been tested for kidney imaging. Exceptionally, gold nanoclusters with the size below 3.5 nm have been validated for real-time imaging of unilateral ureteral obstruction.[20-21] However, it relies on the passive retention of gold nanoclusters in blocked kidneys to obtain a signal readout, and thus fails to delineate the early molecular events at the early stage of kidney injury. We recently reported fluorescent molecular renal probes with positive sensing mechanism that change their signals in response to the biomarkers related to kidney injury.[22] Such probes rely on the respective activation of a single fluorescent moiety, which are unable to detect two interlinked molecular events in the kidneys for imaging of CIAKI. Although coadministration of two different single-channel probes has the potential to imaging two different molecular events simultaneously, different pharmacokinetics of injected single-channel probes could affect their in vivo imaging studies. In contrast, real-time simultaneous imaging of dual biomarkers by using unimolecular duplex reporters not only can provide opportunities to investigate the fundamental correlation between different biomarkers in a certain pathological pathway in living organisms, but also can improve the accuracy of disease diagnosis.[23] However, activatable duplex reporters have been rarely exploited, not to mention used in detection and imaging of CIAKI.[24]

Herein, we report the synthesis of a highly renal-clearable activatable duplex reporter (ADR) for real-time noninvasive chemiluminescence and near-infrared fluorescence (NIRF) imaging of CIAKI in murine model. Because oxidative stress has been well recognized as an early hallmark of CIAKI,[25-26] superoxide anion ($O_2^{\bullet-}$), the primary reactive oxygen species (ROS), is chosen as one of the biomarkers. In addition, upregulation of ROS is known to trigger the pathways towards lysosomal damage and induce the release of the lysosomal enzyme (NAG: *N*-acetyl-β-D-glucosaminidase) from kidney proximal tubular cells,[27-28] NAG is chosen as the other biomarker. Thus, ADR is designed to comprise a $O_2^{\bullet-}$-activatable chemiluminescent signal moiety and a NAG-activatable NIRF moiety, both of which are linked to a renal-clearance scaffold, (2-hydroxypropyl)-β-cyclodextrin (HPβCD) (Scheme 1b).[29] After systemic administration of ADR into living mice, it specifically goes to the kidneys and send back its chemiluminescent and NIRF signals to report $O_2^{\bullet-}$ and NAG levels, respectively. Such an

[*] Dr. J. Huang, Dr. Y. Lyu, Dr. J Li, P. Cheng, Y. Jiang, Prof. K. Pu
School of Chemical and Biomedical Engineering
Nanyang Technological University
70 Nanyang Drive, Singapore 637457 (Singapore)
E-mail: kypu@ntu.edu.sg

Supporting information for this article is given via a link at the end of the document.

independent duplex sensing capability of ADR avoids signal cross-talk, enabling real-time, noninvasive and simultaneous monitoring of two intercorrelated biomarkers in the kidneys of living mice during the onset and progression of CIAKI.

Results and Discussion

Synthesis and characterization. ADR was constructed through the following three main steps (Scheme 1c): (i) synthesis of the *N*-acetyl-β-D-glucosamine-caged NIRF hemi-cyanine substrate **1**; (ii) synthesis of the trifluoromethanesulfonate-caged chemiluminescent phenoxy-dioxetane substrate **7**; and (iii) conjugation of these caged NIRF and chemiluminescent substrates (**1**&**7**) onto the alkyne-functionalized HPβCD. The hemi-cyanine precursor (CyOH) was synthesized by reacting a symmetric cyanine dye (CyCl) with resorcinol *via* a retro-knoevenagel reaction,[30] followed by its reaction with a bromo-glucose derivative to afford the NIRF hemi-cyanine substrate 1. Synthesis of the chemiluminescent substrate 7 started from the phenol precursor 3 by substituting a $O_2^{\bullet-}$-cleavable trifluoromethanesulfonate group on the phenol position,[31] followed by the hydrolysis of an ester bond to afford the carboxylic acid derivative 5. Under ester coupling conditions, 5 was conjugated with 3-azido-1-propanol to give the enol ether precursor 6. This precursor underwent [2 + 2] cycloaddition with singlet oxygen ($^1O_2$) using a photosensitizer (methylene blue) to afford the 1, 2-dioxetane chemiluminescent substrate **7**.[32-35] Finally, both the azide groups on the NIRF substrate **1** and chemiluminescent substrate **7** were consecutively reacted with the alkyne-functionalized HPβCD to afford ADR. MALDI-TOF-MASS assay confirmed that ADR had an average molecular weight of ~2950 Da, proving the conjugation of one NIRF moiety

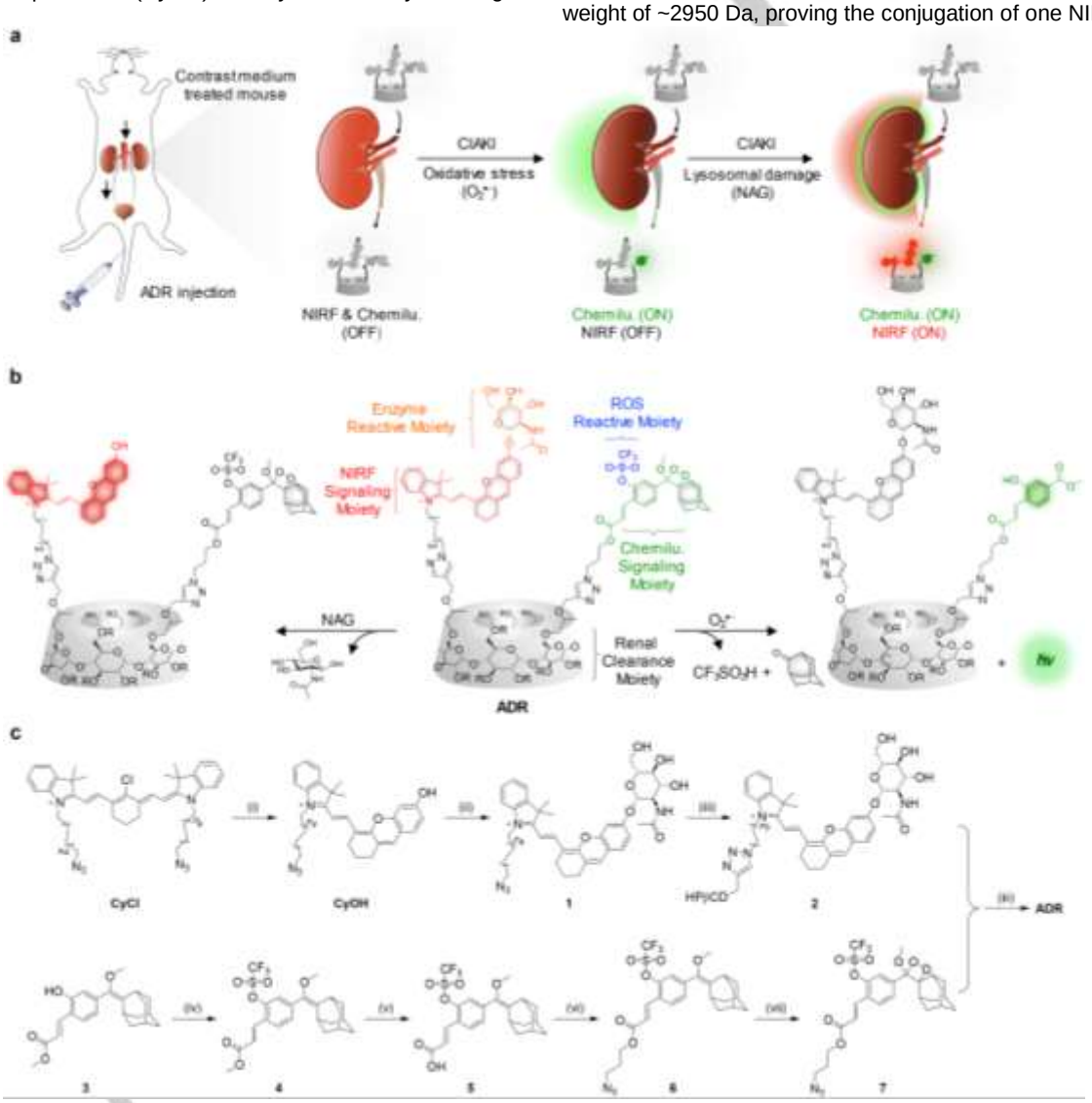

Scheme 1. Design and synthesis of ADR. (a) Schematic illustration of real-time duplex imaging and early detection of CIAKI using ADR. (b) Chemical structures of ADR and its activated forms in response to oxidative stress ($O_2^{\bullet-}$) and lysosomal damage (NAG), respectively (R = H, $CH_2CHOHCH_3$ or CH_2CCH). (c) Synthetic routes for ADR. Reagents and conditions: (i) Resorcinol, K_2CO_3, CH_3CN, 55 °C, 3 h; (ii) Cs_2CO_3, CH_2Cl_2, BrGlcNAc (Scheme S1), 16 h; NaOMe, MeOH, rt, 15 min; (iii) $CuSO_4$•$5H_2O$, sodium ascorbate, propynyl-HPβCD, DMSO/H_2O, 2 h, rt. (iv) Trifluoromethanesulfonic anhydride, pyridine, CH_2Cl_2, -78 to 25 °C, 3 h; (v) KOH, rt,

24 h; (vi) 1-Ethyl-3-(3-dimethylaminopropyl) carbodiimide, 4-Dimethylaminopyridine, 3-azido-1-propanol (Scheme S1), rt, 24 h; (vii) Methylene blue, O_2, CH_2Cl_2/MeOH, 4 h, ice bath.

and one chemiluminescent moiety per HPβCD (Figure S1).

***In vitro* detection.** To study the optical properties and sensing ability of ADR, its absorption, chemiluminescence and NIRF spectra were measured in the absence or presence of $O_2^{\bullet-}$ or NAG. ADR had an absorption maximum at 600 nm and was initially non-fluorescent with a low fluorescent quantum yield of 0.009 in PBS solution, because the fluorophore was in a "caged" state that the electron-donating ability of the oxygen atom was diminished. Upon the addition of NAG, the absorption peak at 600 nm decreased concomitant with the appearance of a new peak at 695 nm (Figure 1a). Meanwhile, ADR showed a 10-fold enhancement in the fluorescence intensity at 720 nm (Figure 1b&S2) and an increased fluorescent quantum yield of 0.18 (Table S1) after incubation with NAG. This was due to the cleavage of glycosidic bond of *N*-acetyl-β-D-glucosamine moiety by NAG, which led to the formation of CyOH moiety with strong electron-donating phenolate group of the fluorophore and thus strong fluorescence. The cleavage of glycosidic bond was further confirmed by observation of a new high-performance liquid chromatography (HPLC) peak at a retention time of 3.1 min corresponding to *N*-acetyl-β-D-glucosamine (Figure 1c). Moreover, the catalytic efficiency (k_{cat}/K_m) of NAG towards ADR was calculated to be 0.025 μM^{-1} s^{-1} (Figure 1d), suggesting its high sensitivity for detection of NAG. Upon addition of $O_2^{\bullet-}$, the absorption and fluorescence spectra of ADR showed negligible change (Figure 1a&1b), while the chemiluminescence at 520 nm increased ~12000-fold (Figure 1e). Such an enhancement should be ascribed to the fact that $O_2^{\bullet-}$ attacks the sulfonate ester group of ADR to cleave trifluoromethanesulfonate, leading to the formation of an unstable phenolate dioxetane intermediate. This intermediate is an active chemiluminescent substrate that spontaneously undergoes decomposition to emit photons.[32-35] The cleavage of trifluoromethanesulfonate and subsequent release of 2-admantanone were confirmed by HPLC, showing a characteristic peak at a retention time of 26.1 min (Figure 1c). Good linearity between the chemiluminescence signal at 520 nm and the KO_2 concentration was observed for ADR, showing an estimated limit of detection (LOD) of 12 nM (Figure 1f). Moreover, the chemiluminescence half-life of ADR was approximately 7.8 min (Figure 1g), and should be long enough for *in vivo* imaging. Note that incubation of ADR with both NAG and $O_2^{\bullet-}$ led to the chemiluminescent spectrum with the maximum at 520 nm, the same as that after incubation with $O_2^{\bullet-}$ alone (Figure S3). This implied no energy transfer from the chemiluminescent moiety to the activated NIRF moiety probably due to their long distance. Nevertheless, ADR had negligible NIRF and chemiluminescence responses towards other interfering analytes including other enzymes, ROS, and metal ions (Figure 1h), suggesting its high specificity of NIRF and chemiluminescence activation channels towards NAG and $O_2^{\bullet-}$, respectively.

To study the ability of ADR to detect $O_2^{\bullet-}$ and NAG in cultured cells, HK2 cells (an immortalized proximal tubule epithelial cell line from normal adult human kidney) were treated with a radiocontrast medium - diatrizoate (DTZ) (100 mg/ml) in medium for 1 h or 5 h. In control groups, cells were treated with PBS or NAC (an antioxidant, N-acetyl L-cysteine, 100 mM) for 1 h prior to co-incubation with mixture of DTZ and NAC for 5 h. All groups were then incubated with ADR (10 μM) for chemiluminescence and fluorescence imaging. The chemiluminescence intensity of DTZ-

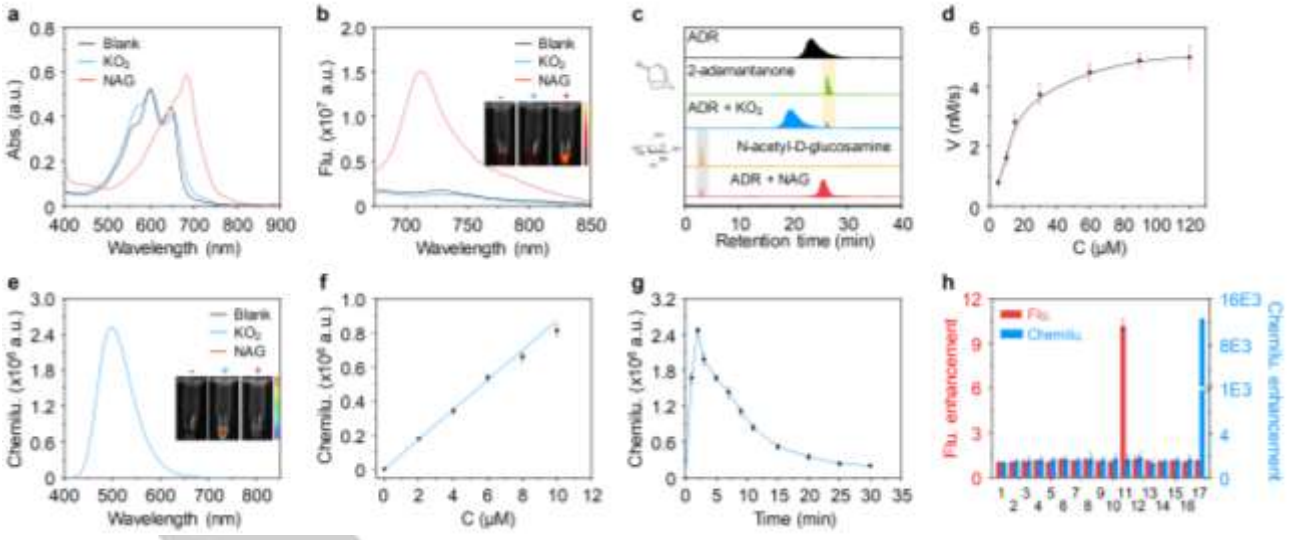

Figure 1. *In vitro* detection of $O_2^{\bullet-}$ and NAG using ADR. (a) UV-Vis absorption and (b) fluorescence spectra of ADR (30 μM) in the absence or presence of KO_2 (60 μM) or NAG (40 mU) in PBS (10 mM, pH 7.4) at 37 °C. Inset: the corresponding fluorescence images acquired at 720 nm upon excitation at 675 nm with IVIS spectrum imaging system. (c) HPLC traces of ADR (30 μM) in the absence or presence of KO_2 (60 μM) or NAG (40 mU), and the traces of pure 2-admantanone as well as *N*-acetyl-β-D-glucosamine for comparison. (d) Steady-state kinetics of the enzymatic reaction between ADR (5, 10, 15, 30, 60, 90 or 120 μM) and NAG (40 mU). (e) Chemiluminescence spectra of ADR (30 μM) in the absence or presence of KO_2 (60 μM) or NAG (40 mU) in PBS (10 mM, pH 7.4) at 37 °C. Inset: the corresponding chemiluminescence images acquired under bioluminescence mode of IVIS spectrum imaging system with the acquisition time of 1s. (f) Chemiluminescence intensities of ADR (30 μM) as a function of the concentration of KO_2 (0-15 μM). (g) Chemiluminescence kinetic profiles of ADR (30 μM) in the

presence of KO_2 (60 μM) in PBS (10 mM, pH 7.4). (h) The NIRF and chemiluminescence changes of ADR (30 μM) at 720 nm and 520 nm, respectively, after incubation with indicated ROS (150 μM), enzymes, and metal ions (150 μM) in PBS (10 mM, pH 7.4) at 37 °C. 1, blank; 2, hydroxyl radical; 3, singlet oxygen; 4, peroxynitrite; 5, hypochlorite anion; 6, hydrogen peroxide; 7, furin; 8, plasmin; 9, β-galactosidase; 10, fibroblast activation protein-alpha; 11, NAG; 12, Na^+; 13, K^+; 14, Mg^{2+}; 15, Fe^{2+}; 16, Ca^{2+}; 17, KO_2. Data in (d) and (f-h) are the mean ± SD. n = 3 independent experiments.

treated cells was 110 and 240-fold higher than the PBS-treated cells at 1 h and 5 h post-treatment of DTZ, respectively; however, when the cells were pre-treated with NAC, chemiluminescence signals decreased to the basal levels (Figure S4), because NAC could scavenge cellular ROS and prevent oxidative stress. In contrast, the NIRF intensity of DTZ-treated cells remained nearly the same as the control. This was due to the fact that although treatment of DTZ induced the release of NAG from lysosomes, the total amount of NAG remained nearly the same in the static cellular condition.[36] Nevertheless, these results confirmed the feasibility of ADR to image $O_2^{\bullet-}$ and NAG in living cells.

Renal clearance and *in vivo* stability studies. To investigate the pharmacokinetics of ADR, the concentration of ADR in the blood was analyzed by HPLC after a single i.v. injection into living mice. Blood concentration curves implied that ADR had a two-compartment profile of *in vivo* kinetics (Figure 2b). The ADR concentration in blood was close to 0 % injected doses (ID) g^{-1} at 115 min post-injection and its elimination half-lives ($t_{1/2\beta}$) was estimated to be 22.02 min, indicating its rapid elimination from the body *via* systemic clearance. The renal clearance of ADR was also examined by HPLC analysis of mouse urine, showing 80.2±4.3% ID at 24 h post-injection in living mice (Figure 2c). After 24 h urinary recovery, the mice were dissected and the residual ADR in the body was determined by HPLC after homogenization of major organs in PBS. The results revealed that the residual ADR (~20%) was mainly accumulated in liver and intestine (Figure 2d), negligible ADR was found in other organs. The renal clearance efficiency of ADR is slightly lower than that of single-channel molecular renal probes in our previous studies,[22] which is attributed to the slightly reduced hydrophilicity after conjugating two fluorophores on one HPβCD. Nevertheless, the renal clearance efficiency of ADR was higher than the ultra- small Pd nanosheets (6.6% ID at 24 h post-injection)[37], gold nanoclusters (52% ID at 24 h post- injection)[20-21] and silica Cornell dots (73% ID at 48 h post-injection)[18], and similar to porphyrin-polyethylene glycol (PEG) (~80% ID at 24 post-injection)[38] and ZW800-CDPL[19] (80% ID at 4 h post-injection)[19]. Such an advantage of ADR was attributed to its high hydrophilicity and low molecular weight (~3 kDa) relative to the glomerular filtration molecular weight cutoff (50 kDa).[39]

To determine *in vivo* stability of ADR, its optical profiles, NIRF images and mass distribution recovered from urine were measured and compared with its pure form in PBS. ADR had almost identical absorption (Figure 2e), fluorescence (Figure 2f&g) and mass spectra (Figure S5) in the urine and PBS, suggesting ADR had negligible *in vivo* metabolism in healthy mice. Moreover, histological and immunofluorescence staining revealed that neither tissue damage nor cellular apoptosis was observed after 24 h injection of ADR, proving its good biocompatibility (Figure S6).

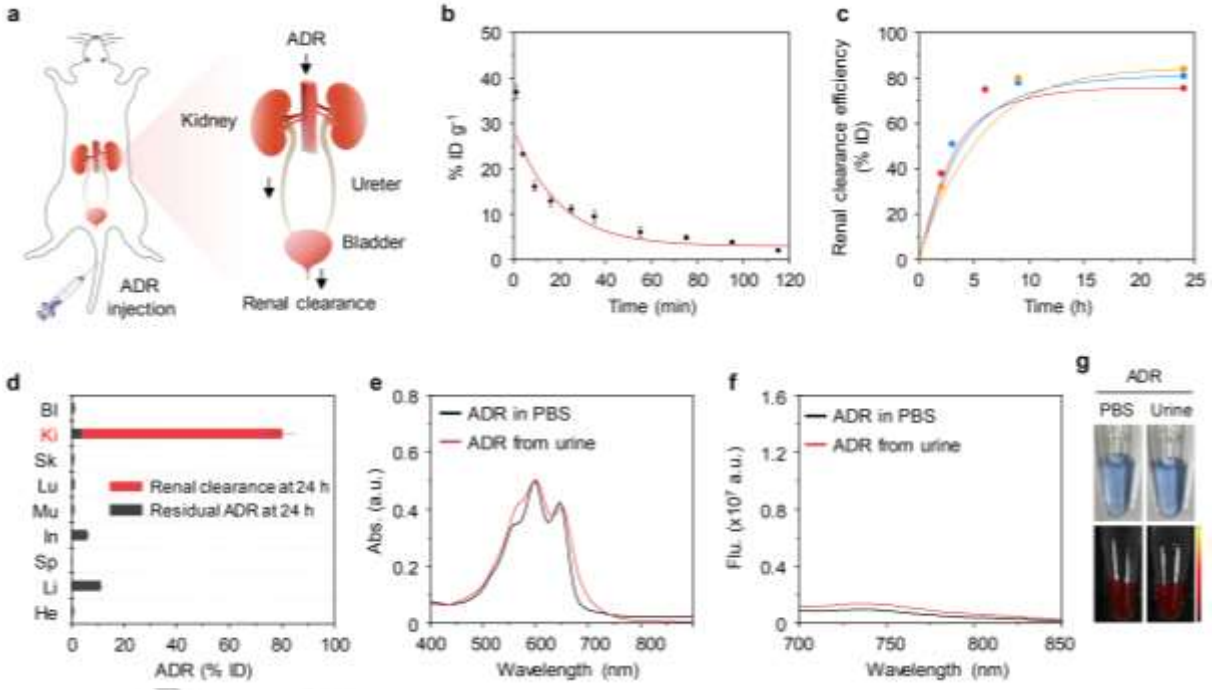

Figure 2. Renal clearance and *in vivo* stability studies of ADR. (a) Schematic illustration of the excretion of ADR through the urinary tract. (b) Blood concentration (% ID g^{-1}) decay of ADR after i.v. injection into living mice. (c) Renal clearance efficiency as a function of time post-injection of ADR (30 μmol kg-1 body weight) in living mice, three lines represent the measurements in three independent mice. (d) HPLC analysis of ADR excreted from kidneys into urine (red bar) and residual ADR in major organs of mice (black bar) after 24 h injection of ADR. Major organs were homogenized in PBS and centrifuged to remove insoluble components. The supernatant containing extracted probes were analyzed by HPLC assay. Heart (He), liver (Li), spleen (Sp), intestine (In), muscle (Mu), lung (Lu), skin (Sk), kidneys

(Ki), bladder (Bl). (e-f) *In vivo* stability studies of ADR using optical characterization. Absorption (e) and fluorescence (f) spectra of ADR in PBS and the urine samples after 24 h i.v injection of ADR and excretion from living mice. (g) White light and NIRF images of ADR in PBS and ADR in the urine excreted from living mice after 24 h i.v. injection of ADR. The corresponding NIRF images acquired at 720 nm upon excitation at 675 nm with IVIS spectrum imaging system. Data in (b) and (d) are the mean ± SD. n = 3 independent experiments.

***In vivo* duplex imaging of CIAKI.** The ability of ADR for real-time duplex imaging of CIAKI was evaluated in the mouse model using DTZ as the model drug, which was a radiocontrast medium with known nephrotoxicity. DTZ was i.v. injected into living mice at a nephrotoxic dosage (1 g kg^{-1}),[40] followed by i.v. injection of ADR at different timepoints post-treatment of DTZ (2, 8, 16, and 24 h). The control group mice were treated with PBS or a nephroprotective antioxidant NAC (10 mg kg^{-1} day^{-1}, i.p. injection) 3 days prior to DTZ administration.[41] Whole-body longitudinal chemiluminescence and NIRF imaging were simultaneously conducted at different post-treatment timepoints (Figure 3a). At 2 h post-treatment of DTZ, the chemiluminescent signal of ADR in the kidneys was close to the control mice throughout the entire imaging course (Figure 3b&3e). However, at 8 h post-treatment of DTZ, the injection of ADR led to a gradual signal increase in the kidneys with a maximum signal observed at 8 min post-injection of ADR (Figure S7). At this timepoint, the kidneys of living mice were clearly delineated with chemiluminescence imaging (Figure 3e), showing an ~2.2-fold signal increase relative to the control mice (Figure 3b). The signal decrease of ADR in the kidneys at later imaging timepoints was caused by its rapid clearance and short elimination half-life (Figure S7c). At 16 h

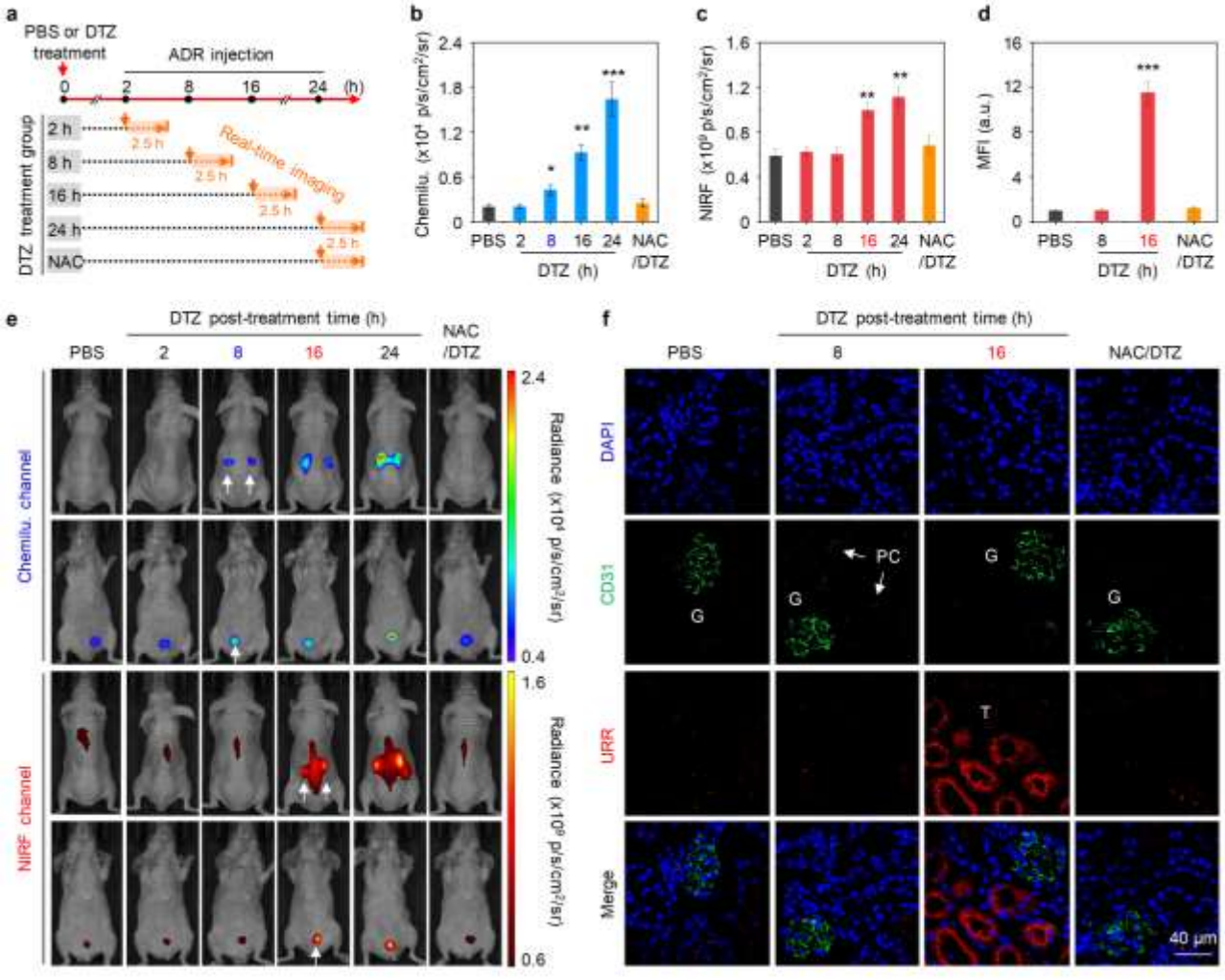

Figure 3. *In vivo* real-time duplex imaging of CIAKI. (a) Schematic illustration of development of CIAKI mouse model and imaging at different post-treatment timepoints. DTZ (1 g kg^{-1} body weight) was intravenously administered into living mice, followed by i.v injection of ADR (30 μmol kg^{-1} body weight) at different timepoints post-treatment of DTZ (2, 8, 16, or 24 h). The control groups were treated with PBS or a nephroprotective antioxidant NAC (10 mg kg^{-1} day^{-1}, i.p. injection) 3 days prior to DTZ administration. Real-time chemiluminescence and NIRF imaging were performed for 2.5 h after i.v. injection of ADR. (b) Chemiluminescent and (c) NIRF intensities of kidneys in living mice at t = 8 or 60 min after injection of ADR at the different post-treatment timepoints. Data are the mean ± SD. n = 6 independent mice. Two-tailed student's t-test. PBS versus DTZ-treated groups, *p<0.05, **p<0.01, ***p<0.001. (d) Mean fluorescence intensity (MFI) of fluorescence microscopy images of kidney sections from mice treated with PBS, 8 or 16 h post-treatment of DTZ, or NAC prior to DTZ administration in panel (f). Data are the mean ± SD. n = 3 independent samples. PBS versus DTZ-treated groups, ***p<0.001. (e) Representative chemiluminescent and NIRF images of living mice at t = 8 or 60 min after injection of ADR at different post-treatment timepoints. The white arrows indicate the kidneys and bladder in the dorsal and ventral side, respectively.

Chemiluminescent images acquired under bioluminescence mode with the acquisition time of 180 s and NIRF images acquired at 720 nm upon excitation at 675 nm with IVIS spectrum imaging system. (f) Representative confocal fluorescence microscopy images of kidney sections from mice treated with PBS, 8 or 16 h post-treatment of DTZ, or NAC prior to DTZ administration. The blue and green signals are from 4', 6-diamidino-2-phenylindole (DAPI) and anti-CD31 antibody, which stain the nucleus and glomerulus (or other vasculatures), respectively. The red signal is from the activated ADR. Glomerulus (G), tubules (T), and peritubular capillaries (PC).

and 24 h post-treatment of DTZ, the chemiluminescence signal in the kidneys further increased to 4.6-fold and 8.2-fold relative to the control group, respectively (Figure 3b), indicating the gradual upregulation of $O_2^{\bullet-}$ during the progression of CIAKI. Similar trends were observed for NIRF imaging (Figure 3c&3e), but the earliest timepoint of the first statistically significant signal increase was observed at 16 h post-treatment of DTZ after 60 min injection of ADR (1.7-fold higher than the control mice, Figure 3c&S7), which was 8 h later than chemiluminescence imaging. The NIRF signals of ADR in the kidneys further increased to 1.9-fold relative to the control group at 24 h DTZ post-treatment time, indicating the gradual upregulation of NAG after administration of DTZ. Such activated chemiluminescence and NIRF signals were also observed in the bladder at different post-treatment timepoints as well (Figure 3e). The activation of ADR was further verified by the emergence of a new absorption peak at 700 nm and an ~3-fold enhancement of fluorescence intensity at 720 nm in the urine of living mice at 16 h post-treatment of DTZ (Figure S8). The fact that ADR sensed the upregulation of $O_2^{\bullet-}$ at an earlier timepoint relative to NAG proved that DTZ first induced oxidative stress followed by lysosomal damage, which coincided with the reported toxic mechanism of DTZ.[42] In addition, such early detection capability of ADR was validated in living mice treated with different dosages of DTZ (Figure S9). The ADR offers simultaneous imaging of two interlinked molecular events in the kidneys to detect CIAKI, while the previous single-channel molecular renal probes failed to do so.[22] NAG is normally secreted at a low concentration (<0.03 unit/24 h) into urine in mice.[43] However, NAG dramatically increased in renal tubules and urine (0.5 unit/24 h) after administration of nephrotoxic drugs.[44] Note that the signals in NAC-treated mice were comparable to the PBS-treated mice because NAC had a superb ROS scavenging ability and protects the kidney against nephrotoxic insult.[45]

To confirm that the in-situ activation of ADR in the kidneys, *ex vivo* fluorescence images of kidneys and other extra-renal organs were recorded. Consistent with the NIRF imaging data observed *in vivo*, fluorescence signals were seen only in the resected kidneys and bladder from mice at 16 h post-treatment of DTZ

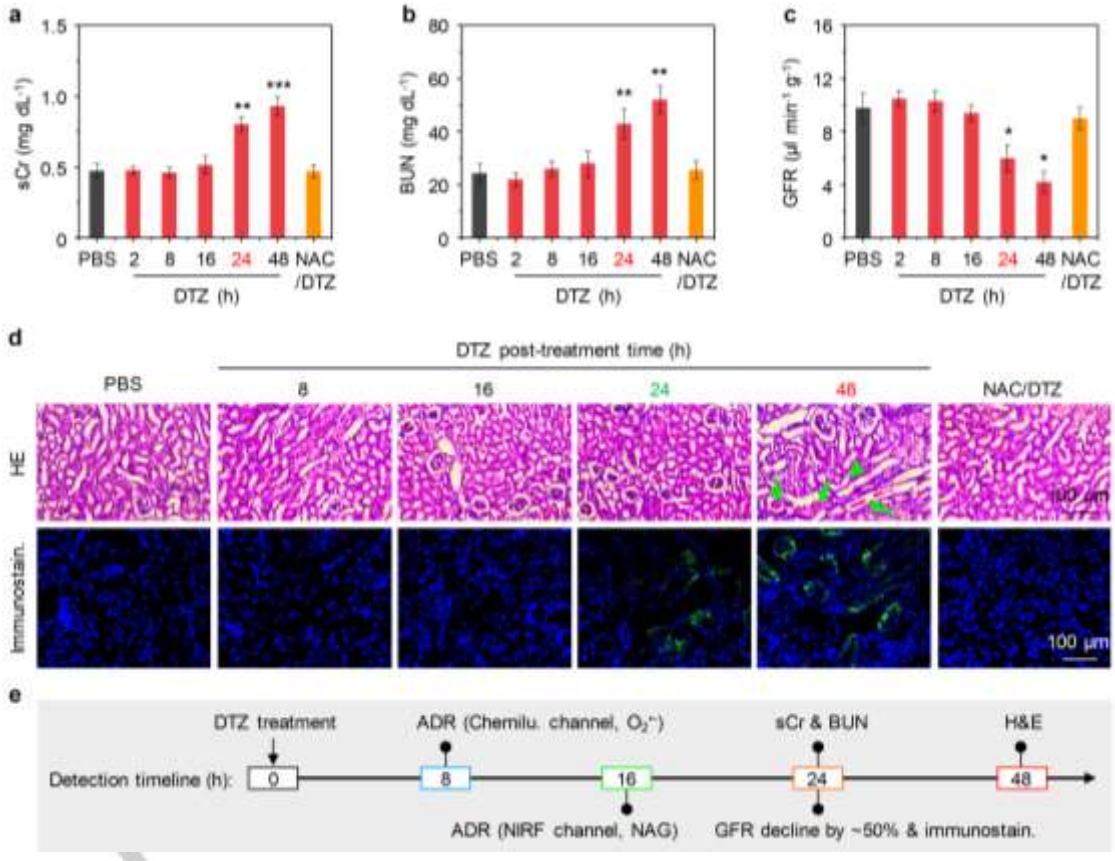

Figure 4. *In vitro* detection of CIAKI with other assays. (a-b) Change in sCr and BUN in living mice after treated with PBS, or NAC prior to DTZ administration, or at t = 2, 8, 16, 24, or 48 h post-treatment of DTZ (1 g kg^{-1} body weight). *Statistically significant differences between PBS and indicated statistically significant timepoints post-treatment of DTZ (*p<0.05, **p<0.01, ***p<0.001, n=3, mean ± s.d.). (c) Determination of GFR in the mouse model of CIAKI. GFR of living mice after treatment of PBS or NAC prior to DTZ administration, or at t = 2, 8, 16, 24, or 48 h post-treatment of DTZ (1 g kg^{-1} body weight), measured by the standard FITC-Inulin assay. *Statistically significant differences in GFR values between PBS and indicated statistically significant timepoints post-treatment of DTZ (*p<0.05, **p<0.01, n=3). (d)

Representative photomicrographs of H&E staining in paraffin embedded kidney sections from mice after treatment of PBS, or NAC prior to DTZ administration, or after treatment of DTZ for 8, 16, 24, 48 h. Green arrows and triangle indicate hyaline casts and loss of the brush border, respectively. (Scale bar = 100 μm). Confocal fluorescence microscopy images of kidney slices from mice after treatment of PBS, or NAC prior to DTZ administration, or after treatment of DTZ for 8, 16, 24, 48 h. The blue and green signals come from DAPI and caspase-3 antibody staining, respectively (Scale bar = 100 μm). (e) Detection timeline of CIAKI comparing ADR (chemiluminescence and NIRF imaging channel) to the clinical and preclinical assays.

(Figure S10&S11), which was 2-fold higher than that of control mice. Moreover, kidney section imaging was performed at different post-treatment timepoints followed by i.v. injection of ADR. The NIRF signal of activated ADR was mainly observed at the kidney tubules rather than the glomeruli at 16 h post-treatment of DTZ (Figure 3f). However, the NIRF signals were undetectable in kidney sections for control mice and mice at 8 h post-treatment of DTZ, which were 10-fold lower than that of 16 h post-treatment of DTZ (Figure 3d). These results were consistent with the fact that DTZ is well known to induce tubular cell damage and result in the release of NAG into tubular lumen.[46]

Comparison with other assays. To compare the detection ability of ADR with the clinical methods, sCr and BUN in the blood of living mice as well as GFR was measured using the commercial assays in DTZ-treated mice. The first statistically significant increase in sCr and BUN was observed at 24 h post-treatment of DTZ (Figure 4a&4b), which was 1.7-fold and 1.8-fold higher than control groups, respectively. Such increased sCr and BUN levels were attributed to the decline in kidney function. This was further confirmed by the observation of ~40% and further ~60% decreases in GFR at 24 h and 48 h post-treatment of DTZ (Figure 4c and Figure S12), respectively, and a reduced clearance rate of ADR at 24 h post-treatment of DTZ (Figure S13). Histological hematoxylin and eosin (H&E) staining showed normal tubular morphology at 24 h post-treatment of DTZ, but the loss of the brush border and hyaline casts at 48 h post-treatment of DTZ (Figure 4d). Moreover, immunofluorescence caspase-3 staining revealed that cell apoptosis was observed for the kidneys at 24 h and 48 h post-treatment of DTZ (Figure 4d).

Comparison of ADR-based imaging and plasma/histological methods in terms of the earliest detection timepoints for CIAKI detection was summarized in Figure 4e. The first statistically significant signal change of ADR-based chemiluminescence imaging occurred at least 16 h earlier than both sCr/BUN assays, GFR measurement, and immunofluorescence caspase-3 staining, and up to 40 h earlier than H&E staining assays. Moreover, ADR-based NIRF imaging outperformed those assays by at least 8 h and up to 32 h. Therefore, these data not only highlighted that ADR-based real-time imaging is more sensitive than sCr/BUN assays and histological analysis, but also validated that $O_2^{\bullet-}$ and NAG were sequentially upregulated prior to GFR decline and kidney tissue damage.

Conclusion

We synthesized a dual-channel optical probe (ADR) that turned on its chemiluminescence and NIRF in the presence of $O_2^{\bullet-}$ and NAG, respectively, and applied it for real-time *in vivo* imaging and early detection of CIAKI. ADR not only had high sensitivity and specificity towards both biomarkers, but also possessed a high renal clearance efficiency (80% ID after 24 h injection), minimal *in vivo* metabolism and high biocompatibility. Systemic administration of ADR into living mice enabled real-time duplex imaging of two correlated molecular events (oxidative stress and lysosomal damage) associated with kidney injury. Such an active sensing mechanism allowed ADR to detect CIAKI prior to GFR decline and renal tissue damage, outperforming the typical clinical plasma assays/preclinical assays by at least 8 h earlier. Thus, ADR holds great promise for screening of safe contrast media in pre-clinical settings and early diagnosis of CIAKI in clinics. To the best of our knowledge, ADR represents the first small molecule probe that not only rapidly clears renally but also specifically activates both chemiluminescence and fluorescence signals to report the dysregulation of dual biomarkers in living animals.

Acknowledgements

This work was supported by Nanyang Technological University (Start-up Grant: M4081627) and Singapore Ministry of Education Academic Research Fund Tier 1 (RG133/15 M4011559, 2017-T1-002-134-RG147/17) and Tier 2 (MOE2016-T2-1-098).

Keywords: molecular imaging • fluorescent probes • biosensor • contrast media • acute kidney injury

[1] L. S. Chawla, P. W. Eggers, R. A. Star, P. L. Kimmel, *N. Engl. J. Med.* **2014**, *371*, 58-66.
[2] P. A. McCullough, *J. Am. Coll. Cardiol.* **2008**, *51*, 1419-1428.
[3] A. D. Calvin, S. Misra, A. Pflueger, *Nat. Rev. Nephrol.* **2010**, *6*, 679-688.
[4] M. Fähling, E. Seeliger, A. Patzak, P. B. Persson, *Nat. Rev. Nephrol.* **2017,** *13*, 169-180.
[5] A. Zuk, J. V. Bonventre, *Annu. Rev. Med.* **2016**, *67*, 293-307.
[6] B. J. Barrett, P. S. Parfrey, *N. Engl. J. Med.* **2006**, *354*, 379-386.
[7] F. Priem, H. Althaus, M. Birnbaum, P. Sinha, H. S. Conradt, K. Jung, *Clin. Chem.* **1999**, *45*, 567-568.
[8] A. Lacquaniti, F. Buemi, R. Lupica, C. Giardina, G. Murè, A. Arena, C. Visalli, S. Baldari, C. Aloisi, M. Buemi, *Radiology* **2013**, *267*, 86-93.
[9] C. Briguori, G. Visconti, N. V. Rivera, A. Focaccio, B. Golia, R. Giannone, D. Castaldo, F. De Micco, B. Ricciardelli, A. Colombo, *Circulation* **2010**, *121*, 2117-2122.
[10] J. W. Pickering, Z. H. Endre, *Am. J. Physiol. Renal. Physiol.* **2016**, *311*, F717-F721.
[11] A. J. Shuhendler, K. Pu, L. Cui, J. P. Uetrecht, J. Rao, *Nat. Biotechnol.* **2014**, *32*, 373-380.
[12] a) Q. Miao, C. Xie, X. Zhen, Y. Lyu, H. Duan, X. Liu, J. V. Jokerst, K. Pu, *Nat. Biotechnol.* **2017**, *35*, 1102-1110; b) Y. Jiang, J. Huang, X. Zhen, Z. Zeng, J. Li, C. Xie, Q. Miao, J. Chen, P. Chen, K. Pu, *Nat. Commun.* **2019**, *10*, 2064; c) J. Li, K. Pu, *Chem. Soc. Rev.* **2019**, *48*, 38-71; d) Q. Miao, K. Pu, *Adv. Mater.* **2018**, *30*, 1801778; e) X. Zhen, J. Zhang, J. Huang, C. Xie, Q. Miao, K. Pu, *Angew. Chem. Int. Ed.* **2018**, *57*, 7804-7808; *Angew. Chem.* **2018**, *130*, 7930-7934; f) P. Cheng, J. Zhang, J. Huang, Q. Miao, C. Xu, K. Pu, *Chem. Sci.* **2018**, *9*, 6340-6347; g) J. Zhang, X. Zhen, J. Zeng, K. Pu, *Anal. Chem.* **2018**, *90*, 9301-9307.
[13] G. Hong, A. L. Antaris, H. Dai, *Nat. Biomed. Eng.* **2017**, *1*, 0010.
[14] D. T. Quang, J. S. Kim, *Chem. Rev.* **2010,** *110*, 6280-6301.

[15] Y. Yang, Q. Zhao, W. Feng, F. Li, *Chem. Rev.* **2012,** *113*, 192-270.
[16] J. Chan, S. C. Dodani, C. J. Chang, *Nat. Chem.* **2012,** *4*, 973-984.
[17] H. S. Choi, W. Liu, P. Misra, E. Tanaka, J. P. Zimmer, B. I. Ipe, M. G. Bawendi, J. V. Frangioni, *Nat. Biotechnol.* **2007,** *25*, 1165-1170.
[18] A. A. Burns, J. Vider, H. Ow, E. Herz, O. Penate-Medina, M. Baumgart, S. M. Larson, U. Wiesner, M. Bradbury, *Nano lett.* **2008,** *9*, 442-448.
[19] H. Kang, J. Gravier, K. Bao, H. Wada, J. H. Lee, Y. Baek, G. El Fakhri, S. Gioux, B. P. Rubin, J. L. Coll, H. S. Choi, *Adv. Mater.* **2016,** *28*, 8162-8168.
[20] B. Du, X. Jiang, A. Das, Q. Zhou, M. Yu, R. Jin, J. Zheng, *Nat. Nanotechnol.* **2017**, *12*, 1096-1102.
[21] M. Yu, J. Zhou, B. Du, X. Ning, C. Authement, L. Gandee, P. Kapur, J. T. Hsieh, J. Zheng, *Angew. Chem. Int. Ed.* **2016**, *55*, 2787-2791; *Angew. Chem.* **2016**, *128*, 2837-2841.
[22] J. Huang, J. Li, Y. Lyu, Q. Miao, K. Pu, *Nat. Mater.* **2019**, *18*, 1133-1143.
[23] P. Cheng, Q. Miao, J. Li, J. Huang, C. Xie, K. Pu, *J. Am. Chem. Soc.* **2019**, *141*, 10581-10584.
[24] Y. Lv, D. Cheng, D. Su, M. Chen, B. C. Yin, L. Yuan, X. B. Zhang, *Chem. Sci.* **2018,** *9*, 7606-7613.
[25] S. N. Heyman, S. Rosen, M. Khamaisi, J. M. Idee, C. Rosenberger, *Invest. Radiol.* **2010**, *45*, 188-195.
[26] A. Pisani, E. Riccio, M. Andreucci, T. Faga, M. Ashour, A. Di Nuzzi, A. Mancini, M. Sabbatini, *Biomed. Res. Int.* **2013**, *2013*, 868321.
[27] W. K. Han, G. Wagener, Y. Zhu, S. Wang, H. T. Lee, *Clin. J. Am. Soc. Nephrol.* **2009**, *4*, 873-882.
[28] M. Andreucci, T. Faga, E. Riccio, M. Sabbatini, A. Pisani, A. Michael, *Int. J. Nephrol. Renovasc. Dis.* **2016**, *9*, 205-221.
[29] J. Huang, S. Weinfurter, C. Daniele, R. Perciaccante, R. Federica, L. Della Ciana, J. Pill, N. Gretz, *Chem. Sci.* **2017,** *8*, 2652-2660.
[30] Q. Miao, D. C. Yeo, C. Wiraja, J. Zhang, X. Ning, C. Xu, K. Pu, *Angew. Chem. Int. Ed.* **2018,** *57*, 1256-1260; *Angew. Chem.* **2018**, *130*, 1270-1274.
[31] J. J. Hu, N. K. Wong, S. Ye, X. Chen, M. Y. Lu, A. Q. Zhao, Y. Guo, A. C. Ma, A. Y. Leung, J. Shen, D. Yang, *J. Am. Chem. Soc.* **2015**, *137*, 6837-6843.
[32] N. Hananya, A. Eldar Boock, C. R. Bauer, R. Satchi-Fainaro, D. Shabat, *J. Am. Chem. Soc.* **2016**, *138*, 13438-13446.
[33] O. Green, T. Eilon, N. Hananya, S. Gutkin, C. R. Bauer, D. Shabat, *ACS Cent. Sci.* **2017**, *3*, 349-358.
[34] S. Gnaim, A. Scomparin, A. Eldar-Boock, C. R. Bauer, R. Satchi-Fainaro, D. Shabat, *Chem. Sci.* **2019**, *10*, 2945-2955.
[35] J. Cao, R. Lopez, J. M. Thacker, J. Y. Moon, C. Jiang, S. N. S. Morris, J. H. Bauer, P. Tao, R. P. Masonc, A. R. Lippert, *Chem. Sci.* **2015**, *6*, 1979-1985.
[36] D. Robic, M. Bens, F. Loko, A. Vandewalle, R. Bourbouze, *Toxicology* **1995,** *103,* 37-44.
[37] S. Tang, M. Chen, N. Zheng, *Small* **2014,** *10*, 3139-3144.
[38] H. Huang, R. Hernandez, J. Geng, H. Sun, W. Song, F. Chen, S. A. Graves, R. J. Nickles, C. Cheng, W. Cai, J. F. Lovell, *Biomaterials* **2016**, *76*, 25-32
[39] A. Ruggiero, C. H. Villa, E. Bander, D. A. Rey, M. Bergkvist, C. A. Batt, K. Manova-Todorova, W. M. Deen, D. A. Scheinberg, M. R. McDevitt, *Proc. Natl. Acad. Sci. U S A* **2010**, *107*, 12369-12374.
[40] C. M. Erley, N. Heyne, K. Burgert, J. Langanke, T. Risler, H. Osswald, *J. Am. Soc. Nephrol.* **1997**, *8*, 1125-1132.
[41] M. Colbay, S. Yuksel, I. Uslan, G. Acarturk, O. Karaman, O. Bas, H. Mollaoglu, M. Yagmurca, O. A. Ozen, *Exp. Toxicol. Pathol.* **2010**, *62*, 81-89.
[42] Z. Z. Liu, K. Schmerbach, Y. Lu, A. Perlewitz, T. Nikitina, K. Cantow, E. Seeliger, P. B. Persson, A. Patzak, R. Liu, *Am. J. Physiol. Renal. Physiol.* **2014,** *306*, F864-F872.
[43] X. Liu, W. Wang, G. Song, X. Wei, Y. Zeng, P. Han, D. Wang, M. Shao, J. Wu, H. Sun, G. Xiong, S. Li, *PLoS One* **2017,** *12,* e0182558.
[44] R. M. Franke, A. M. Kosloske, C. S. Lancaster, K. K. Filipski, C. Hu, O. Zolk, R. H. Mathijssen, A. Sparreboom, *Clin. Cancer Res.* **2010**, *16,* 4198-4206.
[45] S. Fishbane, *Clin. J. Am. Soc. Nephrol.* **2008**, *3*, 281-287.
[46] R. Hofmeister, A. S. Bhargava, P. Gunzel, *Toxicol. Lett.* **1990**, *50*, 9-15.

Entry for the Table of Contents

RESEARCH ARTICLE

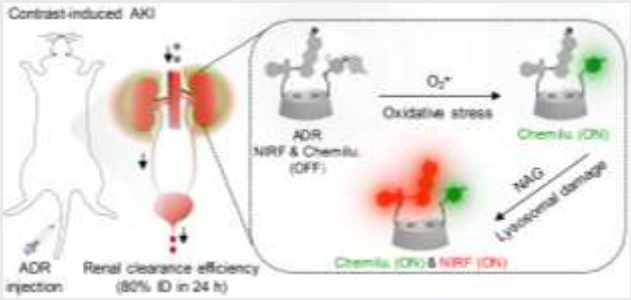

*Jiaguo Huang, Yan Lyu, Jingchao Li, Penghui Cheng, Yuyan Jiang, and Kanyi Pu**

Page No. 1 – Page No. 8

Renal-Clearable Duplex Optical Reporter for Real-time Imaging of Contrast-induced Acute Kidney Injury

A dual-channel optical probe that turns on its chemiluminescence and near-infrared fluorescence in the presence of superoxide anion and N-acetyl-β-D-glucosaminidase, respectively, is synthesized. The probe has a high renal clearance efficiency, enabling real-time in vivo imaging and early detection of contrast-induced acute kidney injury.